Three-dimensional force calibration of a single-beam optical gradient trap

Paul Bartlett and Stuart Henderson[1]

School of Chemistry, University of Bristol, Bristol BS8 1TS, UK

E-mail: P.Bartlett@bristol.ac.uk

Abstract
We have used a high-resolution back-focal-plane detector to make simultaneous measurements of the axial and lateral force constants of a micron-sized particle in a single-beam optical gradient trap. We measure the optical force applied to the trapped particle as a function of the relative index of refraction of particle and medium, the radius of the particle, and the laser beam power. Results are compared with recent theoretical predictions.

1. Introduction

In 1986 Ashkin and co-workers [1] reported the first experimental demonstration of the three-dimensional trapping of a dielectric particle using the radiation pressure from a single, highly focused laser beam. Since then, the single-beam gradient trap (or 'optical tweezer' as it has become known) has become an indispensable tool in biology, chemistry, and colloid physics [2–5] for manipulating single colloidal spheres or cellular organelles such as chloroplasts [6] and nuclei within cells. Trapping techniques have also been extended to encompass macromolecules by tethering large biopolymers such as λ-DNA or protein molecules between the surfaces of two dielectric spheres, and then moving the two spheres using optical forces. Although optical tweezers were used, at first, only to fix or manipulate the positions of particles, in the last few years optical traps have been developed as highly sensitive force transducers [2, 7, 8]. The three-dimensional trapping potential generated by a tightly focused laser beam is, for small particle displacements from the centre of the trap, approximately harmonic in nature. So the force acting on a particle may be determined from the displacement of the trapped particle from its resting position in the trap. Several laser interferometric and photodiode position detection techniques have been developed [7–10]

---

[1] Present address: Australian Radiation Protection and Nuclear Safety Agency, Lower Plenty Road, Yallambie, Victoria 3085, Australia.

which yield the position of the trapped particle with nanometre resolution at high speeds (10^4–10^5 s^{-1}) and allow the quantitative measurement of piconewton or even femtonewton forces. Applications include force generation by single-molecular motors [2, 3], mechanical properties of biopolymers such as DNA [11], titin [12], membranes [13], colloidal interactions [5], and measurement of thermal forces to probe the microscopic rheology of materials [14].

Most optical tweezer applications have, apart from a few studies [10, 15], exploited only one or two dimensions of the optical trap. Forces have been determined either along one axis or in a 2D plane perpendicular to the propagation of light. However, to measure molecular forces and positions in space precisely it is essential to be able to measure the magnitude of forces in all three dimensions. 3D force measurements could allow, for instance, the direct characterization of force generation processes occurring within the interior of a live cell or the tracking of diffusion in highly anisotropic materials. However, the problem has been the lack, until recently, of a technique to determine simultaneously both the axial and lateral displacement of a trapped particle. The earliest position detectors relied on either interference between two circularly polarized light beams [16], a photodiode placed behind the condenser [15], or measurement of the two-photon fluorescence emission intensity [17] to measure displacement along a single axis. Simultaneous two-dimensional particle tracking was achieved first by placing a quadrant photodetector in the back-focal plane (BFP) of a condenser lens [7, 9]. This high-resolution position sensor exploits the interference between the unscattered trapping laser beam and light scattered by the trapped particle [9] to provide lateral displacements with nanometre scale sensitivity at bandwidths of up to 100 kHz. Recently, however, in an important development Pralle *et al* [10] demonstrated that a BFP detector could also yield information about the axial position of the trapped sphere. The quadrant photodiode provides three signals. Difference signals from the upper and lower or right and left sets of quadrants provide two lateral coordinates while a sum signal derived from all four quadrants yields the axial (z-) coordinate. In this paper we use BFP interferometry to track the three-dimensional thermal position fluctuations of an optically trapped particle. Analysis yields the axial (k_z) and lateral (k_r) force constants which characterize the three-dimensional force distribution of a single-beam trap. In an extensive set of measurements we characterize the variation of the axial and lateral trapping forces with the particle radius, the relative index of refraction, and the laser power. We compare our experimental measurements with the predictions of a recent theory of optical forces developed by Tlusty *et al* [18]. We find near quantitative agreement between theory and experiment. Our results should aid the development of three-dimensional force measurements. Such methods will be a basic requirement for future single-molecule investigation within living cells.

2. Optical forces

A stable single-beam optical trap is generated by bringing a Gaussian TEM$_{00}$ laser beam of wavelength λ to a near-diffraction-limited focal spot with a large numerical aperture (NA) microscope objective. The radiation forces exerted on a dielectric sphere of radius a can be resolved into two components: a scattering force directed along the direction of the incident light beam and a gradient force which acts as a restoring force directed towards the beam centre in the case where the index of refraction of the particle n_p exceeds that of the medium n_m. The rigorous calculation of the magnitude of the scattering and gradient forces acting on a non-adsorbing sphere is a challenging problem in optics. One needs to solve the Maxwell equations for the electromagnetic field with the appropriate boundary conditions, and then integrate the corresponding Maxwell stress tensor over the surface of the sphere accounting for the highly inhomogeneous electric field generated by tightly focusing a Gaussian beam. The majority of

theoretical calculations to date remain valid strictly only for either very small spheres (dipolar or Rayleigh regime where $a \ll \lambda$) or very large spheres (geometric optics regime where $a \gg \lambda$). For particles much smaller than the laser wavelength λ, the instantaneous electric field across the particle is uniform and the particle may be treated as a simple induced point dipole [1, 19]. In the geometric limit, where the particle size is large compared to λ, the momentum exchange between the laser beam and particle is calculated from the vector sum of the forces from the refraction and reflection of single plane waves that comprise the beam [20]. However, in the intermediate-size regime ($a \approx \lambda$), where most trapping experiments are performed, the predictions of both theories are in qualitative disagreement with experiment [3]. At intermediate sizes diffraction effects are significant and a strongly focused beam must be represented by a large number of Fourier components and then each plane-wave component further expanded in a series of Mie partial waves [21]. This procedure although exact does not yield closed analytic expressions and is consequently difficult to compare with experiment. While considerable effort has gone into predicting optical forces, the agreement between theory and experiment still remains unsatisfactory. Indeed even the parametric trends predicted have not been rigorously tested.

In general, the strength of trapping forces depends both on the geometry of the applied optical field and on the properties of the particle and the surrounding medium. Here we focus only on particle properties, in particular the relative index of refraction $m = n_p/n_m$, and the radius a of the trapping particle. The two limiting theoretical treatments predict very different dependences for variations in these parameters. For small particles where the dipolar approximation is valid, the scattering force is proportional to the scattering cross-section [19] and so increases as the square of the polarizability:

$$\vec{F}_{\text{scat}}(\vec{r}) = \frac{8\pi n_m}{3c}(ka)^4 a^2 \left(\frac{m^2-1}{m^2+2}\right)^2 I(\vec{r})\hat{z}, \tag{1}$$

where $\hat{z}$ is the unit vector in the propagation direction, $k = 2\pi/\lambda$ is the wavenumber in the medium, and $I(\vec{r})$ is the intensity profile. In the limit where $m - 1 \ll 1$ the scattering force scales as $\sim (n_p - n_m)^2 a^6$. In contrast, the gradient force is linear in the polarizability [19]:

$$\vec{F}_{\text{grad}}(\vec{r}) = \frac{2\pi n_m}{c}a^3 \left(\frac{m^2-1}{m^2+2}\right)\vec{\nabla}I(\vec{r}), \tag{2}$$

and so scales as $\sim (n_p - n_m)a^3$ in the limit of small refractive index difference. To model the beam intensity we assume a paraxial Gaussian beam. At a distance z from the focus and a radial distance r from the beam axis (in cylindrical coordinates) the beam intensity is

$$I(\vec{r}) = \frac{2P}{\pi\omega(z)^2}\exp\left[\frac{-2r^2}{\omega(z)^2}\right] \tag{3}$$

where

$$\omega(z)^2 = \omega_0^2\left[1 + \left(\frac{z}{z_0}\right)^2\right], \tag{4}$$

$z_0 = \pi\omega_0^2/\lambda$, ω_0 is the radius of the beam waist in the focal plane, and P is the beam power [19]. The accuracy of the paraxial approximation is dependent on the parameter $s = \lambda/2\pi\omega_0$. For the situation relevant here, where $s \sim 0.2$ (see section 4), Barton and Alexander [22] estimate that the average error in the electric field using the paraxial approximation is $<10\%$. We expect our calculations of the radiation forces to have a comparable level of uncertainty. In the lateral direction, gradient forces only contribute to the optical potential so the radial trap stiffness $k_r = -\partial(\vec{x}\cdot\vec{F}_{\text{grad}})/\partial x$ evaluated at the beam focus is, from equations (2)–(4),

$$k_r = \frac{32P}{3\omega_0^4 c}a^3(n_p - n_m), \tag{5}$$
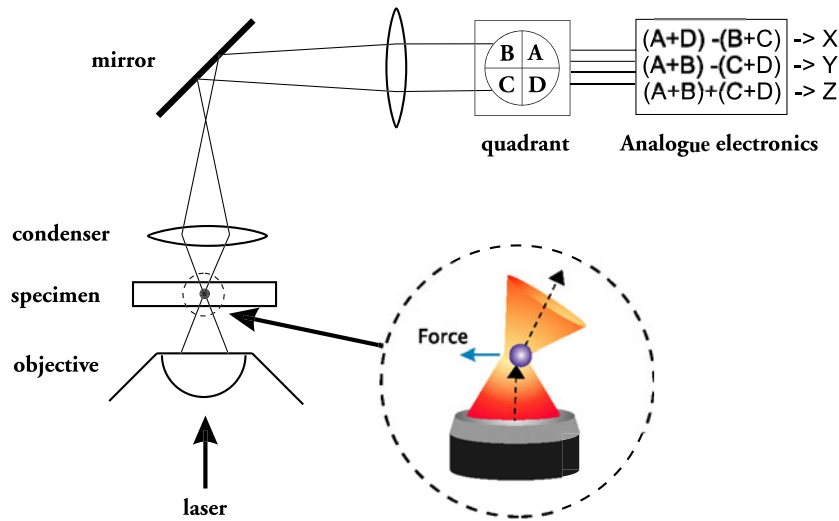
Figure 1. A schematic diagram of the single-beam optical trap and BFP quadrant photodetector.
(This figure is in colour only in the electronic version)

in the limit where $m - 1 \ll 1$. Stable axial trapping requires the gradient forces to exceed the scattering forces. Assuming $\vec{F}_{grad} \cdot \vec{z} \gg \vec{F}_{scat}$, the axial stiffness $k_z = -\partial(\vec{z} \cdot \vec{F}_{grad})/\partial z$ in the dipolar regime is, approximately,

$$k_z = \frac{64P}{3k^2\omega_0^6 c} a^3 (n_p - n_m). \tag{6}$$

We note that the ratio of the axial and lateral trap stiffness, k_z/k_r, is independent of polarizability and is predicted to be a function only of the optical geometry, $k_z/k_r = 2/(k^2\omega_0^2)$. In comparison, there are few quantitative predictions for the trap strengths in the geometric optics regime, where $\lambda \gg a$. Ashkin [20] has shown that the maximal trapping forces increase initially with a rise in the relative refractive index m. However, at high index, scattering forces increase disproportionately in comparison to the gradient forces and the trap becomes ultimately unstable. Since in the geometric optics regime the maximum trapping forces are size independent [23], spring constants are expected to scale inversely with the particle radius a.

3. Materials and methods

3.1. Experimental setup

Figure 1 shows a schematic diagram of the optical tweezer configuration used in this work. The single-beam trap is built around a conventional inverted microscope (Axiovert S100, Zeiss). A diode-pumped Nd-YAG laser (7910-Y4-106, Spectra Physics) with a vacuum wavelength (λ_0) of 1064 nm was used as a light source. The optical trap was produced by focusing the laser in the focal plane with a high-NA (1.3 NA) oil-immersion $100\times$ objective lens (Plan-Neofluar, Zeiss). Transmitted and forward-scattered light was collected by a high-NA oil-immersion condenser lens and the image of the BFP projected onto a quadrant photodetector (QD50-3T, Centronic) via a dichroic mirror. Custom-built analogue circuitry was used to generate difference and sum signals proportional to the x-, y-, and z-positions of the trapped particle. The apparatus was mounted on a vibration-free table.

3.2. Particles

Poly(methyl methacrylate) (PMMA) microspheres were synthesized [24] as test particles. The particles were stabilized against aggregation by a thin layer of a covalently attached comb copolymer of poly(12-hydroxystearic acid) (PHSA) and PMMA. Particle radii were determined using a combination of static and dynamic light scattering and transmission electron microscopy measurements and are accurate to within 2%. The refractive index of the PMMA spheres was estimated to be 1.484 at a wavelength of 1064 nm from the dispersion relation, determined by fitted literature data for PMMA microspheres [25]:

$$n_{\rm p}^2 - 1 = \frac{A_{\rm p}}{1 - (\lambda_{\rm p}/\lambda)^2}, \tag{7}$$

where $A_{\rm p} = 1.1899$ and $\lambda_{\rm p} = 104.4$ nm. The refractive index mismatch $\Delta n = n_{\rm p} - n_{\rm m}$ between particles and medium was varied by suspending the microspheres in a mixture of cyclohexane ($n_{1064} = 1.4184$, density 0.779 g cm^{-3}) and *cis*-decalin ($n_{1064} = 1.4701$, density 0.893 g cm^{-3}). The index of refraction of the solvent mixture was calculated assuming ideal mixing. While the particles are too large for the dipole theory to be valid, for all particle/solvent combinations studied the shift in the phase of light travelling though the particle is sufficiently small, $2ka(m-1) \ll 1$, that scattering from the particles is described accurately by Rayleigh–Gans theory [26] and there is no need for a Mie analysis. The viscosity of the solvent mixture was determined at 25 °C from capillary viscometry measurements. The values measured were numerically fitted to the expression $\eta({\rm mPa\ s}) = 0.436 + 0.489 \exp(1.658w)$, where w is the mass fraction of *cis*-decalin in the mixture. The suspensions of particles (volume fraction, $\phi \sim 7 \times 10^{-5}$) were loaded into thin, rectangular glass capillaries (Vitro Dynamics Inc.) with an internal dimension of 100 μm. The addition of 0.05% PHSA–PMMA copolymer to the suspension media prevented the spheres from sticking to the glass walls of the sample cell.

3.3. Measurement of beam waist

The radius w_0 of the laser beam (the distance in the focal plane at which the intensity has dropped by a factor of $1/\exp(2)$) is an important parameter in the specification of the trapping geometry. To determine w_0 we scanned a PMMA sphere (radius $a = 0.652$ μm) firmly attached to a glass slide back and forth within the focal plane using a piezoelectric stage (P-517 2CL, Physik Instrumente) whilst recording the x- and y-signals from the detector. The detector response was averaged over 100 cycles of a 1 μm sine wave and fitted to the theoretical model proposed by Pralle *et al* [10] to yield values for the beam waist radius w_0 and the x- and y-voltage sensitivities, C_x and C_y (defined by the linear relationship between voltage and displacement, $V = C_x x$ etc). The detector response was found to be linear in particle displacement in an interval of ~200 nm around the trap centre. The beam waist was determined as 0.78 ± 0.1 μm. While the beam waist w_0 did not vary significantly between different runs, we observed much larger variations in the calibration factors which we attributed to slight changes in the exact axial position of the immobilized particle. As a consequence, we did not in general use this technique to calibrate the voltage response of the quadrant detectors.

3.4. Measurement of spring constants

The three-dimensional force distribution was determined from the thermal fluctuations in position of a trapped particle. Before measurement, the particle was moved at least 20 μm above the cover slip to minimize hydrodynamic coupling to boundaries. Under these conditions, hydrodynamic corrections to the Stokes's formula for the viscous drag $\xi = 6\pi\eta a$ on the
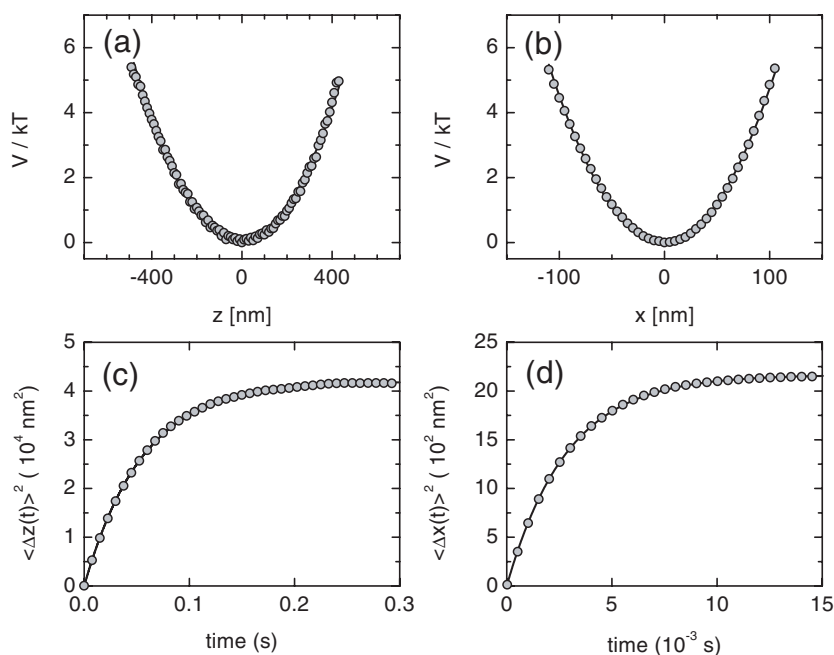
Figure 2. Three-dimensional force calibration. (a) and (b): one-dimensional potentials (in units of $k_B T$) determined from Boltzmann statistics for particle motion in the axial and lateral directions, respectively. Solid curves were obtained by fitting data (see the text) to a harmonic potential, expression (8). The corresponding axial and lateral force constants were $k_z = 2.1 \times 10^{-7}$ N m^{-1} and $k_r = 3.81 \times 10^{-6}$ N m^{-1}. (c) and (d): time evolution of the mean squared displacement in the axial and lateral dimensions, respectively. The theoretical curves (solid) were calculated from equation (11) using $k_z = 2.0 \times 10^{-7}$ N m^{-1} and $k_r = 3.80 \times 10^{-6}$ N m^{-1}. Note the close agreement between the two calibration methods.

particle are less than 2% [27] and were ignored. The laser power was monitored before the beam entered the microscope and corrected to give the power P at the focal region using the transmission of 59% reported by Svoboda and Block [3] for the same microscope objective. The intensity changes at the quadrant photodetector were recorded at 2^{23} time intervals with a sampling rate of 20 kHz (PCI-MIO-16E-4 analogue-to-digital board, National Instruments) and stored on a personal computer for subsequent analysis. The x-, y-, and z-amplitudes of the fluctuations were calculated by subtraction of a mean offset voltage followed by multiplication by the detector sensitivity.

The harmonic nature of the trapping potential was checked by calculating the equilibrium probability $p(l)\,\mathrm{d}l$ of finding the particle between l and $l + \mathrm{d}l$ (where $l = x$, y, or z). The probability distribution function $p(l)$ was normalized by its maximum value. From the Boltzmann law the corresponding potential experienced by the particle is equal to $V(l) = -k_B T \ln p(l)$, where the normalization chosen ensures the potential offset is zero. Curves (a) and (b) in figure 2 show the potential distributions in the axial and lateral directions measured for a 0.643 μm particle trapped in cyclohexane at room temperature (298 K). Temperature effects caused by irradiation with a focused laser beam have been reported to be less than a few kelvins [28], and were consequently neglected in our analysis. The lateral x-potential was accurately fitted by a quadratic potential with a force constant $k_r = 3.81 \times 10^{-6}$ N m^{-1} confirming the harmonic nature of the force distribution for small displacement from the trap

centre. The measured y-potential was also harmonic (data not shown) with a force constant which differed by less than 3% from that in the x-direction. In contrast, the axial probability distribution was clearly asymmetric. We were unable to accurately reproduce the derived axial potential with a quadratic function alone. The solid curve in figure 2(a) shows a fit to the function

$$V(z) = \tfrac{1}{2}(k_z z^2 + F_z z) \tag{8}$$

with an axial force constant $k_z = 2.1 \times 10^{-7}$ N m^{-1} and a linear coefficient $F_z = 4.1 \pm 0.7$ fN (average of five measurements). The presence of this small linear term in the axial potential may be accounted for by a consideration of the gravitational force on the suspended particle. The gravitational minus the buoyant force on the particle is

$$F_g = \frac{4\pi}{3}(\rho_p - \rho_m)a^3 g \tag{9}$$

where ρ_p and ρ_m are the densities of the particle and medium respectively and g is the gravitational acceleration. This axial force acts in opposition to the optical gradient forces and shifts the minimum of the axial potential vertically downwards and with it the position of the experimentally defined $z = 0$ level. Allowing for this shift, it is straightforward to show that the resulting axial potential should be of the form (8) with $F_z = F_g$. The measured density of the PMMA spheres ($\rho_p = 1.166$ g cm^{-3}) gives $F_g = 4.2$ fN, in close agreement to the value measured (4.1 ± 0.7 fN), confirming the origin of the asymmetry seen.

Although the equilibrium Boltzmann analysis confirmed the harmonic nature of the trapping potential, the force constants are more conveniently determined experimentally from a thermal analysis. The dynamics of the trapped particle can be modelled by the Brownian motion of a particle of mass m moving in a three-dimensional ellipsoidal harmonic potential, with axial and radial force constants k_z and k_r, respectively. Particle motion is driven by collisions with molecules of the solvent and damped by the viscosity of the medium. The averaged x-motion of the trapped sphere is, for instance, described by the differential equation

$$m\ddot{x} + \xi\dot{x} + k_r x = (2\xi k_B T)^{1/2}\delta(t) \tag{10}$$

where the drag coefficient ξ is, for a sphere far from a surface, $6\pi\eta a$. This equation is readily solved using Laplace transform techniques. At times long compared to the characteristic times for the momentum relaxation $\tau_B = m/\xi$, the mean squared displacement is given by

$$\langle\Delta x^2(t)\rangle = \frac{2k_B T}{k_r}[1 - e^{-k_r t/\xi}]. \tag{11}$$

To determine the harmonic force constants, the time dependence of the mean squared x, y and z detector signals was evaluated using fast Fourier transform techniques. Since the detector signal is proportional to particle position, the calculated time-dependent voltage fluctuations were fitted to expression (11) to yield the trap stiffness and detector sensitivity. The viscous drag term was calculated from experimental estimates for the viscosity of the trapping medium and the particle radius. Curves (c) and (d) in figure 2 show examples of measured axial and lateral mean squared displacements and their accurate representation by (11). The spring constants found are in good agreement with the values determined from the Boltzmann analysis. Thermal analysis is more convenient experimentally since in contrast to the Boltzmann method it does not require an additional determination of the detector calibration. Accordingly, thermal analysis was used for the remainder of this work.

4. Results and discussion

We have determined the three-dimensional nature of the optical gradient forces on poly(methyl methacrylate) spheres as a function of the relative index of refraction m and particle radius.
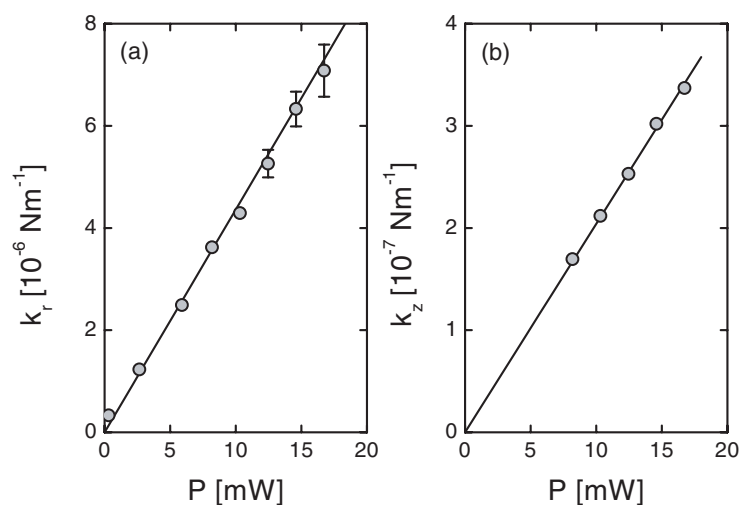
Figure 3. Linear dependence of lateral (a) and axial force constants (b) as a function of laser beam power for 0.643 μm radius PMMA particles suspended in cyclohexane.

The majority of our detailed measurements were made on 0.643 μm radius spheres. First we checked that the trap stiffness varied linearly with the power of the trapping beam. The values of the lateral and axial spring constants are plotted in figure 3 as a function of the estimated laser power in the focal plane. Measurements were made on particles (radius 0.643 μm) suspended in cyclohexane ($m = 1.0461$). The trap stiffness plotted at each power is an average of at least three individual measurements. The measured spring constants are clearly directly proportional to the laser power, as expected from trapping theory.

To investigate the dependence of the stiffness on the relative index of refraction we repeated the above measurements on particles suspended in differing proportions of cyclohexane and *cis*-decalin. Seven solvent mixtures were used, with compositions which varied from 100% cyclohexane to 98% (by mass) *cis*-decalin. In this way the relative index of refraction at $\lambda_0 = 1064$ nm was varied between $1.0101 \leqslant m \leqslant 1.0461$ ($0.0148 \leqslant \Delta n \leqslant 0.0654$). The viscosity of the mixed solvents was estimated from capillary viscometry measurements and was in the range $0.93 \leqslant \eta \leqslant 2.92$ mPa s. In each mixture, we measured the axial and lateral force constants for five different laser powers between 8 and 16 mW. The linear dependence of the optical spring constants on laser intensity was checked. Any recorded values which deviated significantly from a linear fit were repeated. The gradient k/P was extracted from a least-squares fit and is plotted in figure 4 as a function of the refractive index of the medium n_m, for both the axial and lateral directions. The measured axial and lateral force constants increase linearly with the refractive index mismatch Δn, as expected from the dipole approximation (equations (5) and (6)), confirming the dominance of the gradient forces in the creation of a stable optical trap. The solid lines in figure 4 depict linear fits which extrapolate to zero axial and lateral trap strengths at a medium refractive index n_m of 1.485 ± 0.001, in excellent agreement with the refractive index estimated for PMMA spheres at 1064 nm of $n_p = 1.484$. Although the dipole approximation is not expected to be valid for the particle sizes considered here, it is informative to make a quantitative comparison between the current data and its predictions. From figure 4 the gradient $P^{-1}\,dk/dn_m$ is $-6.4 \pm 0.4 \times 10^{-3}$ and $-4.4 \pm 0.2 \times 10^{-4}$ N m^{-1} W^{-1} for the lateral and axial dependence, respectively. The values calculated from equations (5) and (6) are factors of 3–4 times larger than the values measured and reveal the inadequacy of the dipole approximation for spheres with $a \sim \lambda$.
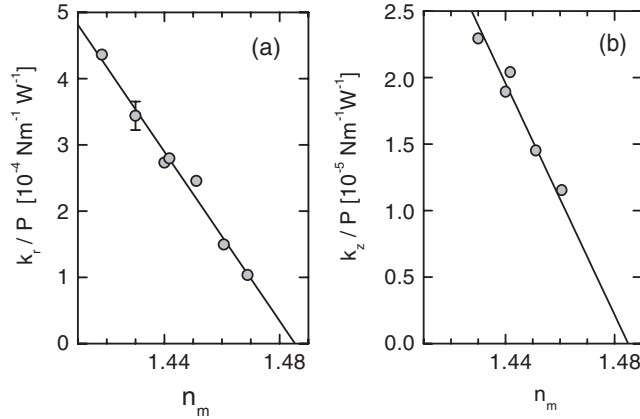
Figure 4. Power-normalized lateral (a) and axial (b) force constants, k_r/P and k_z/P, as a function of the refractive index of the medium n_m at $\lambda_0 = 1064$ nm. The straight lines represent linear least-squares fits. 0.643 μm radius PMMA particles were suspended in mixtures of cyclohexane and *cis*-decalin to vary n_m and the laser powers ranged from 8 to 16 mW.

The optical gradient forces for intermediate-sized particles have been modelled recently by Tlusty *et al* [18]. They argue that the dominant contribution to trapping forces is the rapid variation of the beam intensity around the trapped particle and not interference effects. Ignoring phase factors, they treat the particle as a collection of dipoles and using a simple Gaussian model derive closed expressions for the force–displacement curve. Differentiation yields an analytic expression for the lateral force constant:

$$k_r/P = k_0 a_c \, \mathrm{erf}\left(\frac{a_c}{\sqrt{2}}\right) \mathrm{erf}\left(\frac{a_c}{\sqrt{2}\epsilon}\right) \mathrm{e}^{-(1/2)a_c^2}, \tag{12}$$

where the particle is approximated by a cube of the same volume[2]. Here $a_c = \frac{2a}{\omega_0}(\frac{\pi}{6})^{1/3}$, the eccentricity ϵ defines the dimension of the beam waist in the axial direction [18], and the prefactor k_0 is chosen such that, in the limit where $m - 1 \ll 1$ and $a \ll \omega_0$, equation (12) reduces to the Rayleigh result (equation (5)). This gives $k_0 = 4(n_p - n_m)\epsilon/c\omega_0$. In the geometric optic limit ($a \gg \omega_0$) equation (12) has an incorrect limit, k_p decaying as $\mathrm{e}^{-a_c^2/2}$ rather than as $1/a_c$ as expected, but the differences are probably not significant for the particle sizes considered here. Applying expression (12), using the experimentally determined values for the Gaussian beam waist ($\omega_0 = 0.78$ μm) and particle size, gives a value for the lateral gradient $P^{-1}\,\mathrm{d}k/\mathrm{d}n_m$ as -8×10^{-3} N m^{-1} W^{-1} which is quite similar to the value measured ($-6.4 \pm 0.4 \times 10^{-3}$ N m^{-1} W^{-1}). The eccentricity ϵ was estimated from the paraxial Gaussian model (3) as $\epsilon = 8.2$. The closeness of this agreement, with no adjustable parameters besides ω_0 and ϵ, is very encouraging and suggests that the Tlusty model provides an accurate description of trapping forces for these particle sizes.

Further discrepancies with the predictions of a dipole model are revealed by the dependence of the trap strength on the particle radius. Particles of six different radii ranging from 424 to 921 nm were studied. Lateral force constants were determined at four different laser beam powers between 9 and 25 mW. Dispersions were studied in cyclohexane only. The values of the power-normalized trap stiffness k_r/P are plotted in figure 5. k_r/P increases at first, reaching a broad maximum where $a \sim 500$ nm, before finally decreasing with increasing radius. A

---

[2] We have used the approximate expressions for the trapping force (equations (4) and (5) of [18]) rather than the analytic expression given for the trap stiffness (equation (8)) which seems to have a typographical error.
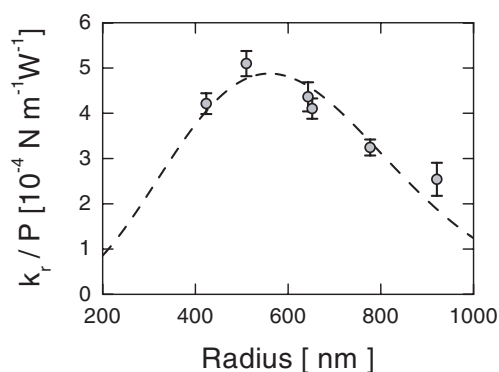
Figure 5. Power-normalized lateral force constant k_r/P as a function of particle radius. The theoretical curve (dashed curve) was obtained from a least-squares regression fit to expression (12), adjusting the prefactor k_0 and beam waist ω_0, and using $\epsilon = 8.2$. The fitted parameters were $k_0 = 8 \times 10^{-3}$ N m^{-1} W^{-1} and $\omega_0 = 0.6$ μm.

similar dependence has been reported by Simmons *et al* [8] who rationalized the non-monotonic behaviour as reflecting the transition between the a^3-increase predicted by dipole theory and the a^{-1}-decrease expected from geometric optics. The dashed curve in figure 5 depicts a least-squares fit to the Tlusty predictions (12), varying both the beam waist ω_0 and the prefactor k_0 to allow for small systematic uncertainties in the data. Again agreement is very reasonable considering the rather limited number of radii studied and confirms the accuracy of the Tlusty model. In general we find that the discrepancies between experiment and the Tlusty model are of order 20–30%, which may perhaps be fortuitous given the strong dependence of the lateral force constants on ω_0^4. Although the fitted values for ω_0 and k_0 differ from experimental estimates, the discrepancies are relatively small. For instance, the fitted values for $\omega_0 = 0.6$ μm and k_0 of 8×10^{-3} N m^{-1} W^{-1} are to be compared with experimental estimates of 0.78 μm and 9×10^{-3} N m^{-1} W^{-1}, respectively.

Finally, the mechanism of the BFP detection technique used here to track the position of the trapped particle depends on a far-field interference between the incident laser beam and the light scattered by the trapped particle [9]. The momentum transferred from the light beam to the particle in this process is the physical origin of the radiation forces which are exploited in an optical trap. The common underlying mechanism implies a link between trapping forces and detector response. During the course of our measurements we noticed that laser intensity, refractive index, and particle radius had very similar effects on the detector sensitivity to the changes seen in the force constants and discussed above. In figure 6 the experimentally determined detector sensitivity is plotted as a function of the force constant, for both the lateral and axial directions. The data were collected from measurements made on 0.643 μm particles under a wide variety of laser powers and refractive index differences. It is clear that detector sensitivity and the optical spring constant are linearly related with a constant of proportionality which does not vary with either particle polarizability or beam intensity. Consequently, the BFP signal is best interpreted not as revealing particle position but as tracking directly the time-dependent optical force applied to the particle. The linear relationship between sensitivity and trapping forces is implicit in the model of the BFP detector described by Gittes and Schmidt [9]. From their analysis it is straightforward to show that the lateral sensitivity C_r has the form $C_r = (\beta k c \omega_0/\sqrt{\pi}) k_r$, where β is the detector voltage generated for a unit-power incident beam. For the current set-up, the output voltage was measured as $\sim$83 V W^{-1} laser power at
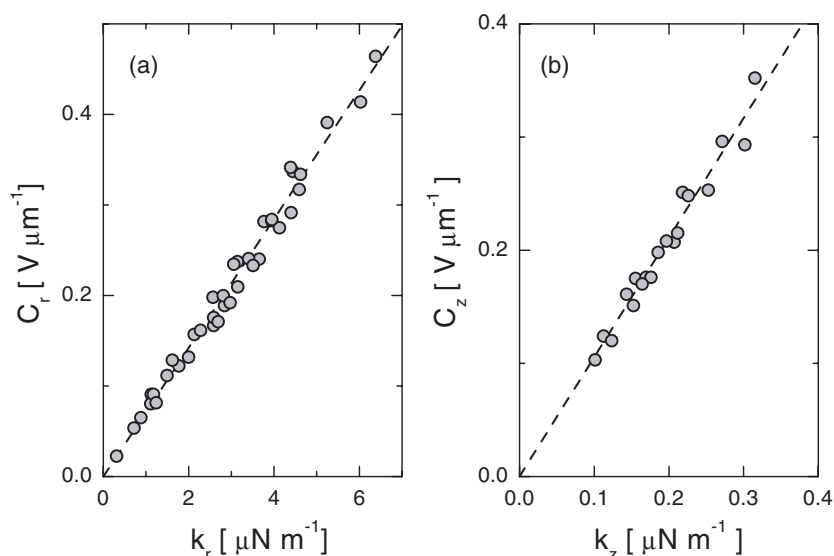
Figure 6. Quadrant detector sensitivity for particle displacement along (a) the lateral and (b) the axial axis as a function of the trap force constant measured under identical conditions. The experimental data were collected at four laser intensities and in at least five different solvent mixtures. The dashed line depicts the best-fit linear relationship.

the detector, implying a lateral force sensitivity $C_r/k_r \sim 9 \times 10^{10}$ V N^{-1}. This value is in close agreement with the gradient of the line plotted in figure 6(a) ($C_r/k_r \sim 7 \times 10^{10}$ V N^{-1}) and confirms that the BFP interferometry signal records directly the force exerted on a particle trapped in a beam, rather than its position.

5. Conclusions

We have used BFP interferometry to measure the polarizability and size dependences of the axial and lateral trapping forces on a particle in a single-beam optical gradient trap. Although many papers have been published reporting the measurements of trapping forces, there have been few systematic studies of the effect of particle properties on trap efficiency. Here, in contrast to the majority of experiments detailed in the literature (which use micron-sized polystyrene or silica spheres in water), the maximum phase shift $k(m-1)2a$ produced by the particles studied is always smaller than unity. In consequence, the particles are best described by Rayleigh–Gans theory (equivalent to the first Born approximation where the scattering from each volume element within a particle differ only in phase not amplitude [26]), rather than requiring a more sophisticated and complex Mie analysis. The scattered amplitude in the Rayleigh–Gans approximation is found by multiplying the amplitude found from a point dipole (Rayleigh) model by an angle-dependent function $R(\Omega)$ which is unity for forward scattering. The validity of the Rayleigh–Gans approximation considerably simplifies the theoretical calculation of trapping forces [29].

We show experimentally that the strengths of the axial and lateral trapping forces are both linear in the particle polarizability. This observation confirms that in a stable optical trap the gradient force dominates the scattering force, which scales quadratically with the polarizability. Furthermore, we find that the lateral trap stiffness is strongly particle size

dependent. The trapping forces increase with particle radius, reaching a maximum at a radius $a \sim 500$ nm, before decreasing with further increases in size. We compare the results of our experiments with a recent theoretical model introduced by Tlusty *et al* [18]. This simple model emphasizes the strong localization of the optical field near the focus of a beam and calculates the radiation forces on a trapped particle using a point dipole approximation in which each volume element is assumed to scatter independently of its neighbours (equivalent to the Rayleigh–Gans model with $R(\Omega) = 1$). Using parameters derived from experiment, we find near quantitative agreement between this model and our experiments. The model evidently describes accurately the physical factors which govern lateral trapping, at least for the intermediate-sized particles studied in this work ($a \sim \lambda$). Finally, we confirm that a BFP detector tracks quantitatively the actual forces applied to a trapped particle.

Acknowledgments

References

[1] Ashkin A, Dziedzic J M, Bjorkholm J E and Chu S 1986 *Opt. Lett.* **11** 288
[2] Sheetz M (ed) 1998 Laser tweezers in cell biology *Methods in Cell Biology Series* vol 55 (New York: Academic)
[3] Svoboda K and Block S M 1994 *Annu. Rev. Biophys. Biomol. Struct.* **23** 247
[4] Ashkin A 1997 *Proc. Natl Acad. Sci. USA* **94** 4853
[5] Grier D G 1997 *Curr. Opin. Colloid Interface Sci.* **2** 264
[6] Bayoudh S, Mehta M, Rubinsztein-Dunlop H, Heckenberg N R and Critchley C 2001 *J. Microsc.—Oxford* **203** 214
[7] Visscher K, Gross S P and Block S M 1996 *IEEE J. Sel. Top. Quantum Electron.* **2** 1066
[8] Simmons R M, Finer J T, Chu S and Spudich J A 1996 *Biophys. J.* **70** 1813
[9] Gittes F and Schmidt C F 1998 *Opt. Lett.* **23** 7
[10] Pralle A, Prummer M, Florin E L, Stelzer E H K and Horber J K H 1999 *Microsc. Res. Tech.* **44** 378
[11] Brower-Toland B D, Smith C L, Yeh R C, Lis J T, Peterson C L and Wang M D 2002 *Proc. Natl Acad. Sci. USA* **99** 1960
[12] Kellermayer M S Z, Smith S B, Granzier H L and Bustamanta C 1997 *Science* **276** 1112
[13] Helfer E, Harlepp S, Bourdieu L, Robert J, MacKintosh F C and Chatenay D 2001 *Phys. Rev. Lett.* **87** 088103
[14] Gittes F, Schnurr B, Olmsted P D, MacKintosh F C and Schmidt C F 1997 *Phys. Rev. Lett.* **79** 3286
[15] Ghislain L P, Switz N A and Webb W W 1994 *Rev. Sci. Instrum.* **65** 2762
[16] Denk W and Webb W W 1990 *Appl. Opt.* **29** 2382
[17] Florin E L, Horber J K H and Stelzer E H K 1996 *Appl. Phys. Lett.* **69** 446
[18] Tlusty T, Meller A and Bar-Ziv R 1998 *Phys. Rev. Lett.* **81** 1738
[19] Harada Y and Asakura T 1996 *Opt. Commun.* **124** 529
[20] Ashkin A 1992 *Biophys. J.* **61** 569
[21] Neto P A M and Nussenzveig H M 2000 *Europhys. Lett.* **50** 702
[22] Barton J P and Alexander D R 1989 *J. Appl. Phys.* **66** 2800
[23] Wright W H, Sonek G J and Berns M W 1993 *Appl. Phys. Lett.* **63** 715
[24] Antl L, Goodwin J W, Hill R D, Ottewill R H, Owens S M, Papworth S and Waters J A 1986 *Colloids Surf.* **17** 67
[25] Underwood S M and van Megen W 1996 *Colloid Polym. Sci.* **274** 1072
[26] van de Hulst H C 1981 *Light Scattering by Small Particles* (New York: Dover)
[27] Happel J and Brenner H 1965 *Low Reynolds Number Hydrodynamics* (London: Prentice-Hall)
[28] Celliers P M and Conia J 2000 *Appl. Opt.* **39** 3396
[29] Rohrbach A and Stelzer E H K 2001 *J. Opt. Soc. Am.* A **18** 839